An Optical Voltmeter for Studying Cetyltrimethylammonium Interacting with Fused Silica/Aqueous Interfaces at High Ionic Strength†

Patrick L. Hayes, Ehow H. Chen, Jennifer L. Achtyl, and Franz M. Geiger*

Department of Chemistry, Northwestern University, 2145 Sheridan Road, Evanston, Illinois 60208

Received: December 10, 2008; Revised Manuscript Received: February 18, 2009

Electrostatics and counterions play important roles in many supramolecular processes, including surfactant adsorption and aggregation at interfaces. Here, we assess their influence on how the common surfactant cetyltrimethylammonium (CTA) interacts with fused silica/aqueous interfaces by determining thermodynamic, kinetic, and electrostatic parameters for CTA adsorption across a range of NaCl concentrations (10−500 mM NaCl) using second harmonic generation (SHG). Using vibrational sum frequency generation (SFG), we demonstrate that vibrationally resonant contributions and nonresonant background contributions to the SFG signal intensity that depend on the interfacial potential can be quantified simultaneously during the adsorption process, which provides insight into the nonequilibrium dynamics of CTA adsorption. By analyzing the adsorption free energies as a function of interfacial potential at these four salt concentrations, the charge density per adsorbate is determined, indicating that CTA coadsorbs with counterions at a ratio of approximately 4 to 3 (i.e., 4 CTA^+ ions for every 3 Cl^- ion). The chemical (i.e., non-Coulombic) portion of the free energy is found to dominate the overall free energy of adsorption, indicating that CTA adsorption at these ionic strengths is primarily driven by the favorable hydrophobic interactions between interdigitated surfactant hydrocarbon chains in the adsorbed aggregate. By applying Gouy−Chapman−Stern theory to our data, an average charge density of 2.8(3) × 10^{13} charges/cm^2, which corresponds to 0.7 to 1.7 molecules/nm^2, was obtained for the four NaCl concentrations.

I. Introduction

Surfactant adsorption at solid/aqueous interfaces is important in a diverse set of chemical and technological applications, including nanoparticle synthesis and function, fracturing fluids for enhanced oil recovery, and separations.[1−3] Because of its general importance, the interaction of cationic surfactants with aqueous/solid interfaces has been studied extensively. Excellent reviews of this work are available in the literature.[1,4] One commonly studied system is the cetyltrimethylammonium (CTA) cation, a quaternary alkyl ammonium surfactant, at the SiO_2/aqueous interface. Early work relied on depletion measurements, which provided valuable thermodynamic information.[5] More recent techniques such as relectometry,[6] ellipsometry,[7] atomic force microscopy (AFM),[6] quartz crystal microbalances (QCM),[8,9] neutron reflection,[10] sum frequency generation spectroscopy (SFG),[11] and total internal reflection Raman scattering (TIR Raman)[11] have provided much needed information on the kinetics, nanometer-scale morphology, and the molecular-level conformation of CTA at the SiO_2/aqueous interface.

There are only a few studies of quaternary alkyl ammonium surfactant adsorption at high salt concentrations, even though many technological applications require surfactant/salt mixtures with high ionic strengths.[2] Our second harmonic generation (SHG) and broadband sum frequency generation (SFG) studies extend previous work on CTA adsorption at the silica/aqueous interface toward these often industrially relevant ionic strengths. Specifically, we use SHG and SFG to probe CTA adsorption in the presence of four different NaCl concentrations: 10, 100, 300, and 500 mM. In this work we utilize the Eisenthal $\chi^{(3)}$ method, also referred to as the $\chi^{(3)}$ technique, which is an SHG methodology that probes the interaction of charged species with solid/aqueous interfaces in real time, under flow conditions, and with exquisite surface specificity.[12−14] The Eisenthal $\chi^{(3)}$ method provides a wide range of valuable information regarding the thermodynamics, kinetics, and electrostatics of CTA adsorption to silica/aqueous interfaces at high ionic strengths. In the $\chi^{(3)}$ formalism, the SHG signal depends on the interfacial potential and thus surface charge. As the signal is optical, the Eisenthal $\chi^{(3)}$ method is akin to using an optical voltmeter that probes the native system without the need for electrochemical labels. All experiments were carried out at pH 11, where silica has a relatively large and negative surface charge density, with the expectation that adsorption of the cationic surfactant would lead to large positive changes in surface charge density, large changes in SHG signal, and improved signal-to-noise. Complementary vibrational SFG studies were also carried out for CTA adsorbed at the silica/aqueous interface in the presence of 10 mM NaCl to obtain vibrational spectra of CTA in situ without the need for subtracting bulk contributions. Moreover, our work demonstrates that broadband SFG can be used in time-resolved studies to correlate changes in surface charge density with changes in CTA surface coverage during the adsorption process. It is hoped that this analysis, and further SFG studies using the same methodologies, will help elucidate the equilibrium and nonequilibrium dynamics and structures of ionic surfactants at solid/aqueous interfaces.

II. Cetyltrimethylammonium Cations at Solid/Aqueous Interfaces

A. Low Ionic Strength. A general literature survey regarding the interaction of CTA with solid/aqueous interfaces shows that in the absence of excess alkali halide electrolyte, adsorption

† Part of the "George C. Schatz Festschrift".

* To whom correspondence should be addressed. E-mail: geigerf@chem.northwestern.edu.

10.1021/jp810891v CCC: $40.75
Published on Web 03/23/2009

isotherms usually more closely resemble a two-step model, which is defined by four regions.[4−6,11] In region one, which occurs at the lowest CTA concentrations, the surface excess increases as monomers adsorb to negatively charged surface sites through a primarily electrostatic interaction. In region two, the isotherm reaches a plateau due to saturation of charged surface sites. In region three, as the bulk concentration approaches the critical micelle concentration (CMC), a sharp increase is observed in the surface excess, which is attributed to adsorbed aggregate formation, with the previously adsorbed monomer possibly acting as nucleation sites. In region 4, which begins around the CMC, the adsorption isotherm once again levels out as the surface becomes saturated with adsorbed surfactant aggregates. In regions one and two, the surface excess is much smaller than in regions three and four. Additionally, the adsorbed aggregates can adopt either a "worm-like" or round "admicelle" morphology depending on the identity of the counterions and the concentration of CTA.[6] The two-step model is an idealized model and in practice it can be difficult to distinguish experimentally between region one and region two because of the low surface excesses in these regions. The techniques listed above have provided a wealth of valuable information about each step in the CTA adsorption process; however, questions still remain. In particular, AFM studies, which have been the primary source of information about CTA surface morphology,[6] have not been successful characterizing CTA morphology at concentrations much less than the CMC. Herein we utilize SFG, with its unique sensitivity to interfacial symmetry and conformation, to characterize adsobate structure at concentrations inaccessible to AFM.

B. High Ionic Strength. In the presence of excess alkali halide electrolyte (i.e., at higher ionic strengths in excess of approximately 1 mM) the identity and concentration of counterions can dramatically alter the behavior of CTA at the silica/aqueous interface. The influence of counterions depends on the particular system under investigation. For instance, upon addition of KCl or KBr electrolyte, the different regions of the CTA adsorption isotherm become less distinct.[6] Instead of four regions, a more general increase is observed below the CMC, and the isotherm then levels around the CMC. For other ionic surfactants at charged oxide interfaces, a similar "blurring" of the different regions in the adsorption isotherms is observed upon addition of electrolyte.[15] This result is not surprising because when an electrolyte such as KBr is added to the system the free energy of the electrostatic step will be less favorable than in the absence of KBr due to charge screening between the silica surface and cationic surfactant. Moreover, it is expected that surface aggregation would become more energetically favorable because of a decrease in the repulsion between the charged surfactant head groups due to the same charge screening effects. Here, we investigate CTA adsorption at high NaCl concentrations where due to such energetic considerations the different regions in the two-step model are less distinct.

The morphology of the adsorbed aggregates is also influenced by counterions as demonstrated in AFM experiments reported by Velegol and co-workers.[6] At high cetyltrimethylammonium bromide (CTAB) concentrations (10 × CMC), the surfactant was found to form "worm-like" micelles at the silica/aqueous interface. At lower concentrations (0.9 × CMC), short rods and/or spheres were observed. In contrast, only spheres were observed at both concentrations (10 × CMC and 0.9 × CMC) when cetyltrimethylammonium chloride (CTAC) was examined. Addition of 10 mM KCl to CTAC solutions increased the CTA surface coverage as assessed by AFM, but the overall morphology of the adsorbed layer remained unchanged. Given their well-known influence on the CMC of surfactants[4,16] and their importance in electrostatic double-layer theories,[17−19] the influence of counterions on CTA adsorption is not surprising. The role of counterion binding in the formation of bulk CTA micelles has been quantitatively characterized for a variety of systems.[16,20,21] However, with the AFM study previously mentioned in this section as a notable exception, experimental studies on how electrolyte concentration controls CTA adsorption and aggregation have been limited to mostly depletion and ζ-potential measurements, which provide little molecular-level information about adsorbate structure.[1,15,22] To address this knowledge gap we have carried out SHG studies of CTA adsorption that provide not only thermodynamic information about CTA adsorption at high ionic strengths but also structural information such as degree of counterion binding, charge density, and adsorbate number density. On a more general note, counterions play a key role in the behavior of a wide range of supramolecular structures, with one fitting example being the melting transition of comb polymer−DNA hybrids, which was recently studied by Schatz and co-workers.[23] Therefore, we hope this work demonstrates the versatility and utility of SHG and SFG for studying the interplay between ions and macromolecules at buried interfaces.

III. Theoretical Background

A. The Eisenthal $\chi^{(3)}$ Method. SHG is a well-known nonlinear optical technique that is used to probe a variety of interfaces, surfaces, and other noncentrosymmetric systems.[24−27] To track surfactant binding at the silica/aqueous interface, we specifically utilize a variant of SHG that was pioneered by Eisenthal,[28] who named it the $\chi^{(3)}$ technique. Recent work has demonstrated the applicability of the $\chi^{(3)}$ technique for quantifying both the thermodynamics and the electrostatics of metal cation adsorption and protein adsorption at a variety of mineral oxide and organic-containing solid/water interfaces[12−14,29−31] as well as for characterizing DNA-functionalized surfaces.[32,33] In this technique, the dependence of the SHG signal on interfacial potential, Φ_0, is modeled according to eq 1:

$$\vec{E}_{2\omega} \propto \overleftrightarrow{\chi}^{(2)}\vec{E}_{\omega}\vec{E}_{\omega} + \overleftrightarrow{\chi}^{(3)}\vec{E}_{\omega}\vec{E}_{\omega}\Phi_0 \qquad (1)$$

where $E_{2\omega}$ is the second harmonic electric field, E_{ω} is the applied fundamental electric field, and $\chi^{(2)}$ and $\chi^{(3)}$ are the second-order and third-order nonlinear susceptibilities of the interface.[28,34−36] Conceptually, eq 1 attributes the total SH light generated to two contributions. The $\chi^{(2)}$ term is independent of the static electric field and the corresponding electric potential at the silica/aqueous interface. In contrast, the $\chi^{(3)}$ term is modulated by the surface potential and can be attributed, on the molecular level, to the polarization and net orientation of water molecules that are aligned by an interfacial electric field resulting from a charged surface.[29,37] Specifically for this study, the fused silica substrate is expected to carry a net negative surface charge density when in contact with a pH 11 aqueous solution.[19,38,39] The resulting surface potential decays to the bulk value with increasing distance into the bulk solution. In previous work by Eisenthal and co-workers and also by our group, this potential is modeled successfully by using the familiar Gouy−Chapman and Gouy−Chapman−Stern (i.e., triple-layer model) theories as well as the constant capacitance model.[12,14,28,29] In the constant capacitance model, which we will apply because it is most relevant for describing the interfacial potentials set up by the

high charge densities found in this work while avoiding overparametrization, the interfacial potential is the ratio of the net surface charge, σ, and the capacitance of the interfacial region, C, according to[17,19,40]

$$\Phi_0 = \frac{\sigma}{C} \tag{2}$$

Equations 1 and 2 show that changes in the surface potential, and thus the SHG E-field, depend on changes in charge density at the interface. By tracking the changes in the SHG signal intensity (i.e., the square modulus of the SHG E-field expressed in eq 1) that are caused by the interaction of CTA cations with the silica/aqueous interface, we can study the molecular details of adsorption and desorption. The high sensitivity of the method can be attributed to self-heterodyning, with the $\chi^{(2)}$ and $\chi^{(3)}$ terms being the local oscillator and the signal, respectively.[32,41] Assuming Langmuirian adsorption,[39,42,43] the surface charge density will be modulated by the bulk cation concentration according to the approach put forth by Salafsky and Eisenthal:[29]

$$\sigma = \sigma_0 + \sigma_{CTA}\left(\frac{K \times C_{CTA}}{1 + K \times C_{CTA}}\right) \tag{3}$$

In eq 3, σ_0 is the surface charge density of the bare silica/aqueous interface at a given bulk solution pH and electrolyte concentration, σ_{CTA} is the interfacial charge density resulting from adsorbed CTA at surface saturation, K is the equilibrium binding constant from the Langmuir adsorption isotherm, and C_{CTA} is the bulk concentration. Thus, by combining eqs 1−3 we obtain an expression for the SHG signal intensity as a function of CTA concentration. By fitting this model and an analogous model where the potential is represented using Gouy−Chapman−Stern (i.e., triple-layer) theory to our experimental data, we are able to quantitatively determine the binding constants, the free energies of adsorption, the absolute charge density of the interface in the presence of CTA, and information that is crucial to assessing the reversibility of CTA binding to silica/aqueous interfaces. Together with the SFG measurements discussed in the following section, nonlinear optics proves to be a powerful tool for studying the interactions between surfactants and solid/liquid interfaces.

B. Sum Frequency Generation. The theoretical and experimental aspects of sum frequency generation (SFG)[44,45] have been described in detail previously,[26,27,44−51] and thus only a brief summary of the most significant points will be provided here. With incident light fields of sufficient intensity, an IR light pulse and a visible light pulse will couple in a noncentrosymmetric medium, such as an interface, and produce an SFG E-field with a frequency equal to the sum of the IR and visible frequencies without contributions from the centrosymmetric bulk phases. When the incoming IR frequency matches a vibrational mode in an adsorbate, the SFG signal is resonantly enhanced, and by monitoring the SFG signal across a range of IR wavelengths, one obtains an intrinsically surface selective vibrational spectrum. As shown in eq 4, the intensity of the SFG signal, I_{SFG}, is directly proportional to the square modulus of the second-order susceptibility of the interface, $\chi^{(2)}$, and the intensity of the input visible and IR light fields, I_{Vis} and I_{IR}, respectively.

$$I_{SFG} \propto |\chi^{(2)}|^2 I_{Vis} I_{IR} \tag{4}$$

The second-order susceptibility can be expressed as the sum of nonresonant and resonant contributions, $\chi_{NR}^{(2)}$ and $\chi_{Rv}^{(2)}$, respectively (eq 5).

$$I_{SFG} \propto |\chi_{NR}^{(2)} e^{i\gamma_{NR}} + \sum_{\nu=1}^{n} \chi_{R\nu}^{(2)} e^{i\gamma_\nu}|^2 \tag{5}$$

In eq 5, $\chi_{R\nu}^{(2)}$ represents the resonant contribution from each vibrational mode, ν, and γ represents the phase factors associated with both the nonresonant background and the vibrational modes. Furthermore, the resonant contribution to the second-order susceptibility is proportional to the number of resonating surface-bound molecules, N_{ads}, and the molecular hyperpolarizability, β_ν, averaged over all orientations of the molecules (eq 6).

$$\chi_{R\nu}^{(2)} \propto N_{ads}\langle\beta_\nu\rangle \tag{6}$$

The value of β_ν increases when the frequency of the incoming IR pulse matches a vibrational transition of the adsorbate or interface leading to resonance enhancement of the SFG signal. As demonstrated by Eliel et al. with a free electron laser[52] and Richter et al. with a tabletop solid state laser,[51] IR fields that are broad in the frequency domain allow for collection of broadband SFG spectra within a single laser pulse, this approach can be utilized to monitor multiple vibrational modes during the adsorption/desorption process providing information about both the surface coverage and orientation of adsorbates.[51,53−59] Lastly, for the silica/aqueous interface the nonresonant contribution to the SFG signal has, on the molecular level, the same origins as the nonresonant SHG signal used in the $\chi^{(3)}$ technique.[60] Therefore, the nonresonant SFG signal can be modeled following the same theory described for the $\chi^{(3)}$ technique in the previous section.

IV. Experimental Methods

A. SHG and SFG Systems. Our setup for the SHG experiments has been described in detail previously (see Figure S1 in the Supporting Information for a schematic of the experimental apparatus).[41,61−63] Briefly, a regeneratively amplified Ti:Sapphire laser (Hurricane, Spectra Physics, 1 mJ/pulse) pumps an optical parametric amplifier (OPA-800CF, harmonic generator I option, Spectra Physics) at a kHz repetition rate producing tunable laser light between 500 and 750 nm. The $\chi^{(3)}$ experiments were carried out with the laser tuned to ∼635 nm, which is far from any electronic or vibrational resonances in the system under investigation, either at the fundamental or the second harmonic. The laser beam is directed through a variable density filter, where the power is attenuated to 0.5 μJ per 120 fs pulse. After the attenuated fundamental probe light is focused onto the fused silica/aqueous interface, the reflected fundamental and SH light are passed through a UV-grade Schott filter and a monochromator to eliminate the fundamental before the second harmonic light is detected with use of a gated single photon counting system. Unless noted otherwise, all SHG experiments were carried out with a 45-in/s-out polarization combination to eliminate Fresnel factors that are dependent on the interfacial index of refraction.[64] CTA cations adsorb to silica/aqueous interfaces as aggregates approximately 4 nm thick,[4,6] which presumably would change the interfacial index of refraction from that of the bare silica/aqueous interface. Thus, the 45-in/s-out polarization combination is necessary to separate changes in

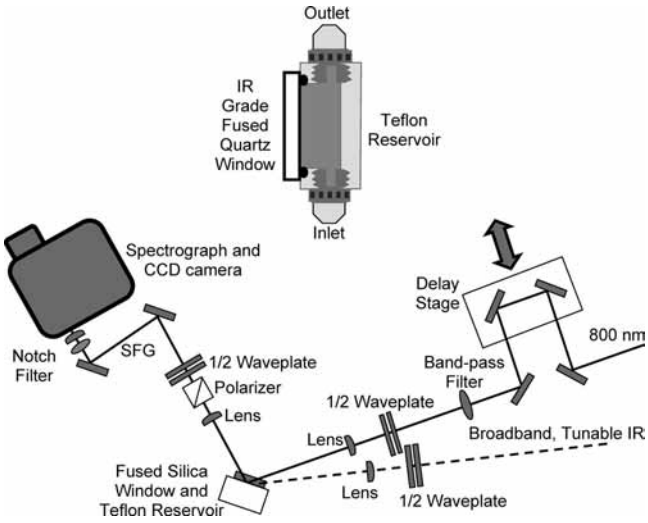

Figure 1. The experimental setup and flow cell used in SFG experiments. See the Experimental Methods section for further details. Top inset: Side view of the flow cell system. For reference, the outlet points up and perpendicular to the laser table. Bottom: Overhead view of the SFG apparatus. Reflected 800 nm and IR beams are omitted for clarity.

SHG signal due to the $\chi^{(3)}$ effect, as expressed in eq 1, from changes in signal due to differences in the Fresnel factors that occur upon CTA adsorption. The quadratic power dependence and appropriate bandwidth of the SHG signal are verified regularly to ensure that the sample damage threshold is not exceeded.

In contrast to the SHG experiments, the SFG work utilizes a different regeneratively amplified Ti:Sapphire laser system (Spitfire Pro, Spectra Physics, 2.5 mJ/pulse) described before.[65,66] Briefly, the laser light passes through a 50/50 beam splitter (Figure 1), and half of the beam is used to pump an optical parametric amplifier (OPA-800CF, difference-frequency mixing option, Spectra Physics) to produce broadband ($\sim$140 cm^{-1} fwhm) IR laser light at a wavelength around 3.4 μm. The IR beam is then directed through an IR waveplate ($\lambda/2$ $CdGaS_4$ 3.1 μm CA 10 mm, Altechna Co. Ltd.) and focused on the silica/aqueous interface by using a BaF_2 (ISP Optics) lens. The remaining half of the original laser beam passes through a time delay stage and a narrow band-pass filter (F1.1-800.0-UNBLK-1.00, CVI) to control timing and provide narrow bandwidth 800 nm pulses. An achromatic half-waveplate (MWPAA2-12-700-1000, Karl Lambrecht Corp.) allows for polarization rotation. The 800 nm and IR beams are focused on to the interface at angles of 45° and 60° from normal, respectively. On the detection side, the polarization of the SFG signal is selected by a polarizer (Glan Laser Polarizer GL15, Thorlabs), after which a half-waveplate (MWPAA2-12-400-700, Karl Lambrecht Corp.) rotates the SFG polarization for optimal throughput to the detector. Then the SFG signal passes through a long-pass filter (600 nm cutoff) and an 800 nm notch filter (Notch Plus Filter, Kaiser Optical Systems, Inc.) to remove light from nonlinear processes other than SFG and reflected 800 nm light. A 0.5 m spectrograph (Acton Research) coupled to a liquid nitrogen cooled, back-thinned charged coupled device (CCD) camera (Roper Scientific, 1340 $\times$ 100 $pixels^2$) is used for signal detection. When measured in-line immediately before the sample, typical pulse energies for the visible and IR beams are 4.0 and 1.5 μJ, respectively.

Spectral fits were carried out by using a custom-written Igor Pro software procedure that convolutes Lorentzians and a nonresonant background. This procedure assumes for vibrational modes to be either in or out of phase with each other (i.e., $\gamma_v = 0°$ or 180°), while treating the phase of the nonresonant background, γ_{NR}, as an independent fitting parameter. Asymmetric stretches are fit 180° out of phase with respect to the symmetric stretches and Fermi resonances.[67,68] SFG peaks were assigned through deuterium substitution studies, comparison to literature assignments, and apparent phase relationships between different peaks in the SFG spectra. All spectra are calibrated to the 2955 cm^{-1} C−H symmetric stretch of the methoxy group in poly(methyl) methacrylate (PMMA).[69] Thin films of PMMA were spin-coated on to an IR grade fused silica window according to our published procedure,[70,71] and PMMA SFG spectra were collected at the silica/air interface with the same experimental geometry and setup used for the CTA studies (i.e., total internal reflection geometry). Background subtraction was performed by using spectra acquired after blocking the IR input, thus accounting for optical scatter from the 800 nm beam. To account for the line shape and intensity profile of the incident broadband IR pulse, all SFG spectra are normalized to the nonresonant SFG spectrum of a gold-coated IR grade fused silica window following Esenturk and Walker.[72]

B. Materials and Sample Cells. All experiments were carried out with use of a custom-built flow cell consisting of, for SHG work, a fused silica hemispherical lens (ISP Optics, UV grade) or, for SFG work, a fused silica window (ISP Optics, IR grade) clamped upon the open top of a Teflon reservoir. A Viton O-ring, cleaned twice daily before and after experiments with Millipore water (18.2 MΩ), is used to seal the substrate to the flow cell and ensure that no leaks occur. All experiments, unless noted otherwise, were performed with a constant flow through the Teflon reservoir. Variable flow peristaltic pumps are used to pump aqueous solutions of CTAB (Calbiochem, 98%), CTAB-d33 (C/D/N Isotopes, 98 atom % D), and NaCl (VWR, 99%) through the flow cell. The flow rate is maintained at $\sim$1.0 mL/s. The pH of all solutions is adjusted to 11 $\pm$ 0.05 through the use of NaOH (Fisher, 98.8%) solutions. Prior to each experiment, the fused silica hemisphere or window was cleaned by successive rinses of Millipore water and methanol followed by sonication in methanol for 6 min. The substrate was then dried in an 100 °C oven for 30 min and finally subjected to 30 s of plasma cleaning in $\sim$1000 mTorr of air. The hemisphere or window was then immediately placed atop the Teflon flow cell or stored under vacuum for up to 6 h before use. After long periods of storage, the hemisphere or window surface was treated with NoChromix (a chromium-free commercial glass cleaner, Godax Laboratories) for 1 h, and then cleaned following the procedure described above. Incomplete deuteration may affect the SFG spectra given that the surfactant is bought commercially with only 98 atom % D. Likewise, some degree of contamination is inevitably present in every aqueous sample, and we determined the total organic carbon in our salt solutions before and after the flow cell to be below 200 ppb (measured with an Apollo 9000 TOC Combustion Analyzer, Teledyne Tekmar, Mason, OH).

C. CTA Quantization by LC-MS. To monitor bulk CTA concentrations during SHG experiments, aliquots from the output flow were collected and analyzed by using LC-MS (Agilent 6210 LC-TOF with Agilent 1200 HPLC introduction). Linear calibration curves were obtained over a CTA concentration range of 15 to 150 μM at each of the four salt concentrations studied in this work (see Figure S2 in the Supporting Informatino for examples of calibration curves). Following procedures given in the literature for quantification of quaternary alkyl ammonium

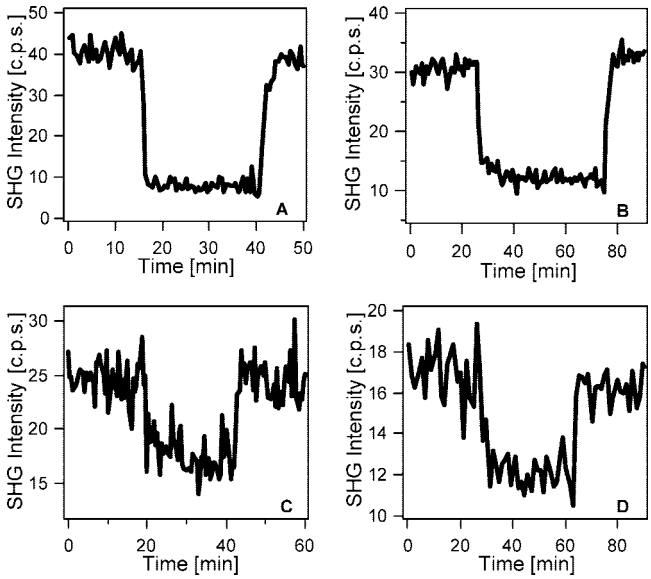

Figure 2. Adsorption/desorption traces observed for CTA binding with the silica/aqueous interface at pH 11 and 295 K, using the following CTA and electrolyte concentrations: (A) 10 mM NaCl, 1 mM CTA, (B) 100 mM NaCl, 1 mM CTA, (C) 300 mM NaCl, 1 mM CTA, and (D) 500 mM NaCl, 0.2 mM CTA.

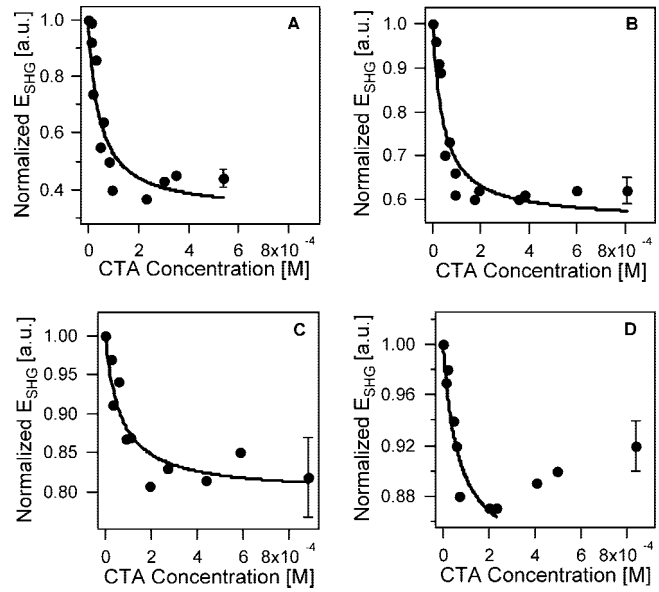

Figure 3. SHG adsorption isotherms for CTA with (A) 10, (B) 100, (C) 300, and (D) 500 mM NaCl as a background electrolyte concentration. Isotherms are measured at pH 11 and 295 K. Each isotherm is composed of data from two identical experiments carried out on separate days. The solid lines represent fits to the data using the $\chi^{(3)}$ equation, in which the potential is expressed by using a constant capacitance model and the CTA adsorption is assumed to follow the Langmuir model. See text for further details regarding fits. All data are normalized to the background aqueous NaCl signal.

surfactants,[73−75] the LC-MS surfactant analysis was carried out in "ESI(+)" mode by using direct injection with a 75%/25% mixture of methanol and formic acid solution (0.2% in H_2O) as the eluent solvent. Peak integrations from either the extracted ion chromatogram (monitoring at *m*/*z* 284.3 for the CTA^+ ion) or the total ion chromatogram (monitoring from 50 to 1500 *m*/*z*) were used for the calibration depending on which provided a more linear calibration. For SFG experiments CTA solutions of a given concentration were prepared beforehand with use of volumetric glassware. NaCl solutions were either prepared by using calibrated glassware or their concentration was measured with a conductivity meter (Fisher Traceable Conductivity and TDS Meter, Fisher Scientific).

V. Results and Discussion

A. Adsorption/Desorption Traces—Time Dependence. To assess the reversibility of CTA binding, we performed adsorption/desorption studies at pH 11 and four different NaCl concentrations by exposing the fused silica/aqueous interfaces to CTA solutions in dynamic flow experiments. With use of our dual-pump flow system, aqueous NaCl solutions are flowed past the silica substrate while monitoring the SHG signal intensity from the interface. At ∼15 min the aqueous NaCl flow is stopped, and simultaneously the CTA flow is started at the same NaCl concentration and flow rate. The SHG signal intensity obtained from the interface in the presence of CTA is monitored until it stabilizes, indicating steady state conditions with respect to adsorption and desorption are met. At this time, the SHG signal intensity is recorded for several more minutes. We then replace the CTA/NaCl flow with a flow of aqueous NaCl at the same concentration used throughout the experiment while continuing the SHG signal collection until the baseline level is reached again, indicating that CTA has desorbed.

The results of the SHG adsorption/desorption experiments for CTA at 10, 100, 300, and 500 mM NaCl are shown Figure 2. (For reference, the CMCs were determined to be $2.2(2) \times 10^{-4}$, $2.6(3) \times 10^{-4}$, $3.8(3) \times 10^{-4}$, and $5.1(5) \times 10^{-4}$ M, respectively, at the four salt concentrations. See Figure S3 in the Supporting Information for details of CMC measurement.) At all four NaCl concentrations, a signal decrease is observed when CTA is brought into contact with the interface. The decrease is consistent with the $\chi^{(3)}$ technique as described in eqs 1−3. The SHG signal returns to the original baseline level when CTA is flushed from the system with NaCl solution, which indicates that the interaction of this surfactant with the fused silica/water interface is fully reversible. The observed reversibility is consistent with reflectometry studies by Velegol et al. (pH 5.6, no salt and 10 mM salt added)[6] and ellipsometry studies by Eskilsson and Yaminsky (pH ∼6, no salt added),[7] although their work was carried out at much lower pH values and ionic strengths.

At 300 and 500 mM NaCl the adsorption traces show dramatically reduced signal-to-noise ratios. Likewise, the SHG signal intensity decreases from 40 to 17 counts per second prior to CTA addition as the NaCl concentration increases from 10 to 500 mM, which is consistent with the notion that for these higher salt concentrations the surface charge is increasingly screened by the NaCl ions, leading to smaller interfacial potentials.[17−19] The lower signal-to-noise ratio is likely due to the smaller changes in interfacial potential resulting from CTA adsorption, which, in turn, lowers the changes in the SHG signal intensity.

B. Adsorption Isotherms. By plotting the SHG *E*-field as a function of bulk CTA concentration at pH 11 and a given salt concentration, quantitative thermodynamic information regarding adsorption can be obtained.[14,29,39] As seen in Figure 3, the SHG *E*-field generally decreases with increasing bulk CTA concentrations at all four NaCl concentrations studied. Each data point in Figure 3 corresponds to a single adsorption/desorption experiment (as described in part A of this section) carried out at the concentration specified along the *x*-axis. Over the course of an adsorption isotherm experiment, the SHG signal for the silica/aqueous interface in the absence of CTA remained nearly constant (less than 5% change) indicating that silica

dissolution over the time scale of the experiment, which is approximately 8 h, does not alter SHG signal intensity levels within our signal-to-noise. At pH 11 and under the ionic strength conditions used in this work, the dissolution rate for quartz is approximately 5×10^{-15} mol cm^{-2} s^{-1}.[76] For 8 h of exposure to the aqueous solution, this rate would then correspond to 9×10^{13} molecules cm^{-2} lost due to dissolution. Therefore, on average a monolayer of silica is lost due to dissolution during an SHG isotherm experiment. Starting with an approximate rms roughness of 2 nm for our polished fused silica hemisphere the material lost could increase surface roughness. However, a rougher surface would be expected to have a lower SHG signal given that the interfacial species would adopt a more isotropic distribution of orientations causing partial cancelation of the SHG response. No decrease in signal is observed over the duration experiment suggesting that increases in surface roughness are not important for the SHG signal intensity, which is consistent with the relatively small amount of material lost due to dissolution when compared to the surface roughness. At all CTA and NaCl concentrations studied, the surfactant concentration was less than 5% of the overall electrolyte concentration in solution. Therefore, the changes in SHG signals observed in both the adsorption isotherms and the adsorption/desorption traces are due to specific interactions between CTA ion and the silica/aqueous interface rather than variation in the background electrolyte.

A fitting equation from which thermodynamic parameters can be extracted is obtained by combining eqs 1−3, and collecting constants.

$$E_{\mathrm{SHG}} = A + B\left(\frac{K \times C_{\mathrm{CTA}}}{1 + K \times C_{\mathrm{CTA}}}\right) \tag{7}$$

In the above, A and B are fitting parameters composed of constants from eqs 1−3. The limitations of the constant capacitance and Langmuir models that are used in deriving eq 7 have been discussed previously.[17,39] However, for analyzing the thermodynamics of adsorption at different NaCl concentrations, we choose the fitting equation given above to avoid overparametrization and fixing values of physical constants a priori (such as the capacitance in the electrical double layer). Fitting our isotherms with a two-step adsorption model is inconclusive, because the different adsorption steps, if they are present, are not resolved. In the Supporting Information the adsorption data are fitted with the Frumkin−Fowler−Guggenheim (FFG) equation[19,42,77] that includes a surface coverage dependent binding constant, which may result from the lateral interactions that are expected to occur between adsorbed surfactants. (See Figures S4 and S5 in the Supporting Information.) In contrast to the FFG equation, the Langmuir model assumes the binding constant is independent of surface coverage. We also apply more sophisticated models for the interfacial potential in this (vide infra) and previous SHG work.[12−14,32,78,79] Fitting eq 7 to the experimental data in Figure 3, equilibrium binding constants of $2.3(8) \times 10^4$, $2.3(6) \times 10^4$, $1.5(5) \times 10^4$, and $1.5(6) \times 10^4$ M^{-1} are obtained for CTA adsorption in the presence of 10, 100, 300, and 500 mM NaCl, respectively (Table 1). The corresponding free energies of adsorption, referenced to 55.5 M water, range from −33 to −35 kJ/mol.[61,62] Figure 3D (500 mM NaCl) shows that in contrast to the other NaCl concentrations, the SHG E-field vs. CTA concentration plot passes through a minimum. This effect was observed in two independent measurements carried out on different days and fused silica samples. One possible explanation is that the adsorbed aggregates undergo a transition from a spherical structure to a "worm-like" structure. It has been shown that, in the presence of 10 mM KCl, CTA forms spherical micelle-like aggregates on silica[6] (n.b., at 500 mM NaCl and the other NaCl concentrations used in this work, any counterion binding by Br$^-$ is small as shown below). However, to the best of our knowledge, the morphology of adsorbed CTA aggregates at high NaCl concentrations and pH values (i.e., near 500 mM and pH 11) has not been previously characterized. Furthermore, it is known that at 1.18 M NaCl bulk CTA micelles undergo a sphere-to-wormlike transition in bulk aqueous systems with increasing surfactant concentration.[16] Therefore, given that high NaCl concentrations drive worm-like micelle formation in the bulk, we tentatively conclude that the observed increase in SHG signal at high NaCl and CTA concentrations is due to the formation of adsorbed worm-like micelles. Accordingly, the fit to the 500 mM NaCl data in Figure 3D is truncated to lower concentrations before this behavior is observed.

TABLE 1: Summary of Binding Parameters for CTA Adsorption to the Silica/Aqueous Electrolyte Interface at pH 11 and 295 K

[NaCl] (mM)	K_{ads} (M^{-1})	$-\Delta G_{\mathrm{ads}}$ (kJ/mol)	initial Φ_0 (mV)[a]
10	$2.3(8) \times 10^4$	35(2)	230
100	$2.3(6) \times 10^4$	34.5(8)	180
300	$1.5(5) \times 10^4$	33(1)	160
500	$1.5(6) \times 10^4$	33(1)	150

[a] Calculated by using the triple-layer model. See text for details.

It should be noted that in the adsorption isotherm experiments as the interfacial potential passes through zero and turns positive with increasing CTA surface coverage the SHG signal will continue to decrease. This conclusion is explained by considering the relative signs of the two terms in eq 1. Before adsorption, or at relatively low surface coverage, the interfacial potential is negative and the two terms have the same sign (n.b., the signs of the two terms in eq 1 are obtained from the adsorption isotherm fits). Thus, the second-order and third-order response constructively interfere with each other. As the magnitude of the interfacial potential decreases (i.e., becomes more positive) with CTA adsorption, the third-order response is diminished, resulting in lower SHG signal. When the interfacial potential passes through zero then the sign of the third-order term changes, and the third-order term begins to partially cancel the second-order term. Therefore, the SHG signal is expected to continue to decrease even as the interfacial potential switches to and becomes more positive. In fact, positive surface charging is observed in our experiments and the interfacial charge densities resulting from the adsorbate are quantified in the next section.

Interestingly, the CTA binding constants at the four salt concentrations show a weak dependence on NaCl concentration that is within the error of our measurements. This similarity in binding affinities indicates that, over the NaCl concentrations studied in this work, CTA adsorption is not dominated by Coulombic interaction between the charged surfactant headgroup and the negatively charged silica/aqueous interface. To further quantify this conclusion, the potential for the silica/aqueous interface without adsorbates was calculated by using the triple-layer model, which was selected due to its appropriateness for predicting changes in interfacial potentials across a wide range of screening electrolyte concentrations.[17] For this calculation, it is necessary to experimentally determine the surface charge density of the silica/aqueous interface at pH 11. Following a

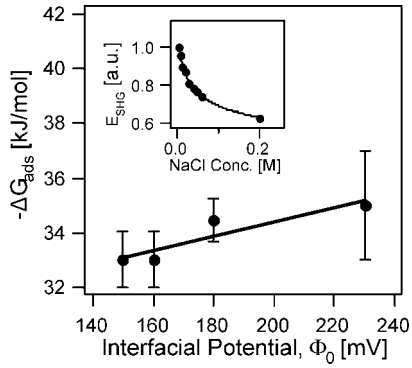

Figure 4. Free energy of CTA adsorption to the silica/aqueous interface plotted versus interfacial potential for the different NaCl concentrations studied. Free energies are determined from the SHG experiments using the Eisenthal $\chi^{(3)}$ method. Interfacial potentials are calculated by using the triple-layer model. See the text for further details regarding the potential calculations. The solid line represents a linear least-squares fit of eq 8 to the data. Inset: $\chi^{(3)}$ charge screening experiment for determination of charge density at the silica/aqueous interface at pH 11. The trace represents the fit of the Gouy−Chapman model to the experimental data.

procedure described by Eisenthal and co-workers,[35,37] SHG was used to measure a surface charge density of −0.019(1) C/m^2, or equivalently, -1.2×10^{13} charges/cm^2 (see Figure 4 inset for experimental data). Furthermore, values of 1.3 and 0.2 F/m^2, which are typical for silica/water and also related oxide/aqueous interfaces, respectively, were used for the capacitance of the inner and β-layers, respectively.[17] Assuming that NaCl does not specifically adsorb to silica, the interfacial potentials are calculated and summarized in Table 1 with the corresponding thermodynamic data. Additionally, in Figure 4 the free energies are plotted against the corresponding interfacial potentials from Table 1. It is common to describe the free energy of adsorption, ΔG_{ads}, as a sum of chemical and electrostatic free energy terms, ΔG_{chem} and ΔG_{elec}, where the electrostatic term can be written as a function of the interfacial potential.[18,19,80]

$$\Delta G_{ads} = \Delta G_{chem} + \Delta G_{elec} = \Delta G_{chem} + \Delta Z F \Phi_0 \quad (8)$$

In eq 8, F is the faraday constant and ΔZ is the change in the charge of the surface species for the adsorption reaction under consideration. A linear least-squares fit of eq 8 to the ΔG_{ads} versus Φ_0 plot in Figure 4 yields a slope of 0.026(9) C/mol and a y-intercept of −29(2) kJ/mol. A ΔZ value of 0.27(9) can be calculated from the slope, indicating that on average 73(9)% of CTA molecules coadsorb with a counterion. This percentage is comparable to the degree of bulk micellar counterion binding reported by Lindman et al. for CTAB and CTAC in water (pH and ionic strength were not controlled in this study, but the pH was presumably 6, and the ionic strength presumably ranged up to 500 mM): approximately 71% for CTAB and 55% for CTAC.[21] Interestingly, our results indicate that even in basic systems, where the number of negatively charged silica surface sites is expected to be relatively high (near 30% of all surface sites),[38] counterions still play an important role in cationic surfactant adsorption. For reference, exchange constants for Cl^- and Br^- binding to CTA micelles reported in the literature indicate that Br^- ions have a higher micelle binding affinity than Cl^- ions.[81] Nevertheless, calculations with these exchange constants show that at the NaCl and CTAB concentrations used in our work counterion binding to the bulk-localized micelles is dominated by Cl^-. Specifically, more than 80% of the anions bound to the bulk-localized micelles consist of Cl^- at 10 mM NaCl, and more than 99.5% of the anions bound consist of Cl^- at 100 mM NaCl.

The y-intercept of −29(2) kJ/mol obtained from the linear fit is the chemical (i.e., non-Coulombic) contribution to the adsorption free energy and is close to the overall free energy for CTA adsorption. It appears that in the range of NaCl concentrations studied here, CTA adsorption is driven primarily by increased hydrophobic interactions between hydrocarbon tails rather than Coulombic attraction between the charged headgroup and negative silica surface sites. The hydrophobic contribution to the adsorption free energy for alkyl ammonium surfactants is approximately 2 kJ/mol per methylene group.[82,83] Thus, the value of ΔG_{chem} obtained from these SHG experiments is equivalent to the participation of 14 or 15 methylene groups per molecule in hydrophobic interactions within the adsorbed aggregate. This result is consistent with the number of methylene groups in the CTA hydrocarbon tail and the notion that adsorbed CTA forms an interdigitated aggregate. Interestingly, the chemical free energy determined in this work is identical with the free energy of aggregation found by Gu et al. using depletion experiments and thermodynamic modeling of CTAB at the silica/aqueous interface without added salt at pH 5.6.[5] This match again supports the notion that CTA adsorption in our experiments is driven by hydrophobic interactions. Given their agreement with previous studies, the thermodynamic values obtained from our experiments indicate that the Langmuir model, while quite simplistic, can be combined with the $\chi^{(3)}$ technique to provide useful information regarding surfactant adsorption. Under the conditions used in this work to measure the adsorption isotherms, CTA surface aggregation occurs simultaneously with electrostatic adsorption in a single step since the two processes are similar energetically. This conclusion is also consistent with the qualitative shape of the SHG isotherms, which lack the "two-step" shape where distinctive regions indicate different steps in the adsorption process.

C. Charge Densities and CTA Surface Density. An advantage of utilizing a more sophisticated model for interfacial potential, such as the triple-layer model, is that one obtains quantitative information regarding interfacial charge densities. However, fitting each data set for a given salt concentration by using the triple-layer model generates unreasonably large errors due to overparametrization in the fitting equation. To circumvent this difficulty, eight separate isotherms (two for each of the four NaCl concentrations) are fitted separately by using the triple-layer model as described in our previously published work.[14] The fits and determined charge densities are displayed in the Supporting Information in Figures S6 and S7, respectively. The charge densities appear to not vary significantly with NaCl concentration. Thus, by averaging these eight independent measurements, a CTA charge density at surface saturation of $2.8(3) \times 10^{13}$ charges/cm^2 is obtained. This value is larger in magnitude than the charge density determined for the silica/aqueous interface in the absence of CTA ($-1.2(1) \times 10^{13}$ charges/cm^2, vide supra). The net positive surface charge density at CTA surface saturation is in agreement with ζ-potential measurements that show negatively charged SiO_2 surfaces become positively charged upon CTA adsorption (no salt was added in these experiments, and although pH is not specified, presumably it was ∼6).[84] The average binding constant determined from the triple-layer fits is $3(1) \times 10^4$ M^{-1}, which, within error, is equal to the binding constants resulting from the previous fits using the constant capacitance model for potential. This consistency suggests that the thermodynamic parameters

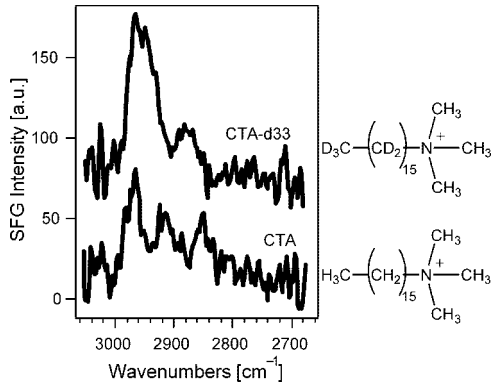

Figure 5. ssp-polarized SFG spectra obtained from the silica/aqueous interface at pH 11 in the presence of 30 μM CTA-d33 (top) or CTA (bottom). All spectra were collected under flow conditions with 10 mM NaCl. The CTA-d33 spectrum is offset for clarity.

determined by using the $\chi^{(3)}$ technique are relatively insensitive to the interfacial potential model selected to fit the data in our system. In section B, we determined that on average 73(9)% of CTA molecules are coadsorbed with a counterion. Therefore, a charge density of $2.8(3) \times 10^{13}$ charges/cm^2 would correspond to a CTA surface density of $1.0(+7/-3) \times 10^{14}$ molecules/cm^2, or, on average, one molecule/nm^2 (the range for one standard deviation is 0.7 to 1.7 molecules/nm^2). These values compare reasonably well with number densities of 2.4(2) molecules/nm^2 reported by Velegol et al. for reflectometry experiments on CTAC in 10 mM KCl and at pH 5.6.[6] The slightly lower value obtained with the $\chi^{(3)}$ technique is likely due to the greater surface roughness of the fused silica hemisphere (2 nm rms roughness or even rougher given dissolution of silica, vide supra) used in our work versus an oxide layer grown on a silicon wafer, which was used in the reflectometry experiments ($\sim$1 nm rms roughness).[6] In related neutron reflection experiments of CTA at the silica/aqueous interface, Fragneto et al. showed that increased surface roughness resulted in lower surface coverage (in these experiments no salt was added and no pH specified, although presumably pH values were close to 6).[10]

D. Vibrational Sum Frequency Generation Spectra. The electronic transitions of CTA are located in the far UV where water absorbs. Thus resonantly enhanced SHG, which is a powerful tool for spectroscopically characterizing adsorbates,[85−89] is difficult to apply to CTA at the silica/aqueous interface. As an alternative, we employ SFG to collect surface-specific vibrational spectra under identical conditions as the SHG experiments. Following the work of Esenturk and Walker,[72] broadband SFG spectra were recorded with four different input IR center frequencies to probe the entire C−H stretching region. Spectra were collected under the same flow conditions used in the SHG experiments, and after CTA was introduced into the flow cell, the system was allowed to equilibrate for 30 min. This length of time was selected based on the equilibration times observed in time-resolved SFG adsorption experiments (vide infra).

Figure 5 shows ssp-polarized SFG spectra obtained from the silica/water interface in the presence of 30 μM CTA at pH 11 and 10 mM NaCl. The notation "ssp" refers to polarization of incident and exigent beams where the first letter refers to the polarization of the SFG light (s-polarized), the second refers to the polarization of 800 nm light (s-polarized), and the third refers to the polarization of the IR light (p-polarized). This polarization combination and the experimental conditions were selected because they provide the greatest signal-to-noise and resolution in the acquired spectra. The top trace in Figure 5 is the SFG spectrum for CTA-d33, where the hydrocarbon tail of the CTA molecule is completely deuterated. (Additional SFG spectra of CTA-d33 over a range of surfactant concentrations are available in the Supporting Information, Figure S8.) The SFG spectrum for the undeuterated CTA molecule is shown in the bottom trace. The CTA-d33 spectrum is assigned first because the spectrum in the C−H region should only contain contributions from the three equivalent methyl groups of the ammonium headgroup, which simplifies analysis. The peaks at 2975 and 2878 cm^{-1} are assigned via spectral fitting to an asymmetric and symmetric stretch, respectively. A shoulder is observed at $\sim$2928 cm^{-1}, which we tentatively assign to the methyl Fermi resonance, although this feature may be due to inhomogeneous broadening of the asymmetric stretch. Additionally, the slightly sloping baseline may be due to water vibrational resonances at higher wavenumbers, although this signal is quite weak due to the well-know property of surfactants and salts to disrupt interfacial water structure and thereby lower its contribution to SFG spectra, as demonstrated recently by Schroedle and Richmond as well as Bain and co-workers.[11,90] The C−H stretching peaks reported here are generally observed in Raman and IR absorbance studies,[11,91,92] and this present work unambiguously probes the surface-bound methyl groups of the ammonium headgroup by using CTA-d33. Certainly, further deuterium substitution and vibrational spectra computed by using algorithms that do not rely on the local mode approximation will aid in spectral assignments. Assigning the 2975 cm^{-1} mode to an asymmetric CH stretch in our SFG work is at variance with the assignment from infrared and Raman work, which treat this mode as a symmetric CH stretch. Spectral fitting of our coherent SFG spectrum with a symmetric mode results in a poor fit, whereas fitting of our coherent SFG spectrum with an asymmetric mode results in a good fit. Spectra fitting thus leads us to assign the 2975 cm^{-1} mode to an asymmetric CH stretch of the ammonium methyl headgroup. Note that this mode analysis by spectra fitting cannot be carried out with spectra recorded with use of noncoherent spectroscopy because the modes in such spectra are not coupled to one another through phase relations. To our knowledge, deuteration studies for spectral assignments of CTA cations in the CH stretching region have not been available until now. Deuteration is important to assess the degree of mode coupling in the SFG spectra of CTA and provides vastly simplified vibrational mode structure.

The undeuterated CTA spectrum is more complex but can be interpreted with the aid of the CTA-d33 spectrum. New peaks at 2919 and 2856 cm^{-1} are observed, which are consistent with the asymmetric and symmetric methylene modes, respectively, and are previously assigned in the literature.[11,91,92] The asymmetric and symmetric modes of the methyl group on the hydrocarbon tail, along with the symmetric and Fermi resonance of the methyl groups on the ammonium headgroup, are not clearly resolved. However, similar to the deuterated spectrum, the asymmetric mode of the ammonium methyl group is observed at 2975 cm^{-1}. The difference in the peak shape for this mode when comparing the CTA-d33 and CTA spectra is due to interference between the vibrational modes of the methylene and the methyl groups in the fully hydrogenated CTA molecule. The destructive interference between the different modes also explains the lower signal-to-noise observed in the CTA spectrum. In recent work, Tyrode et al. studied CTAB interaction with silica/water interfaces at the pH of pure water (i.e., 5.6) and at ionic strengths determined by the CTA concentration (up to 2 mM)[11] and reported that C−H stretching modes were not observed in SFG. This finding was attributed

to the centrosymmetry of the aggregates formed by adsorbed CTA. The cancelation of oppositely oriented dipoles is a well-known effect in second order coherent vibrational spectroscopies, such as SFG, where oppositely oriented modes of the same or similar resonant frequency destructively interfere.[27] Our experiments were carried out under higher salt concentrations (10 mM NaCl) and more basic conditions (pH 11) than in the work by Tyrode et al.[11] The substantially higher interfacial potential of the fused silica/water interface under these different experimental conditions is likely to remove the equivalence of oppositely orientated vibrational C−H modes, therefore giving rise to the vibrational SFG spectral signatures reported here. This situation is comparable to that reported by Schrödle and Richmond,[90] who reported vibrational SFG spectra of dodecanoate at the positively charged fluorite/water interface, which displayed intense C−H stretch contributions.

E. Sum Frequency Generation Adsorption Traces. Following the same theory describing the $\chi^{(3)}$ technique, the nonresonant background in SFG spectra is expected to be proportional to the interfacial potential. Therefore, in principle, broadband SFG can simultaneously probe electrostatics and vibrational resonances as adsorption occurs.[90] However, in practice implementing this parallel analysis requires careful assessment of the time-resolved spectra.

First, the relative phase between the nonresonant and resonant *E*-fields needs to be known. This first challenge is addressed by fitting eq 5 to the relatively straightforward CTA-d33 spectrum and obtaining a relative phase of −115(6)° between the resonant asymmetric methyl stretch *E*-field and the nonresonant background *E*-field. Second, the nonresonant signal is ideally measured in a spectral region with negligible contributions from resonances. This second challenge is addressed by centering the broadband IR pulse at ∼2975 cm^{-1} and measuring the resonant SFG signal from the asymmetric methyl stretch of the ammonium headgroup at 2975 cm^{-1} and the nonresonant signal at 3000 cm^{-1}. We selected conditions (pH 11, 10 mM NaCl, and 30 μM CTAB) where, as shown in Figure 5, the resonant contributions to the SFG signal from CTA and water are relatively small at 3000 cm^{-1}, thus allowing for estimation of the nonresonant signal. From Figure S9 in the Supporting Information we obtain a largely flat line within the signal-to-noise in the SFG spectrum when normalizing SFG spectra of the fused silica/water interface at pH 11 to the SFG spectrum of a gold substrate. Using this figure, we can estimate the resonant contribution at 3000 cm^{-1} is roughly 5% of the total SFG signal level observed for the silica/aqueous interface before exposure to the surfactant. Therefore, we treat the SFG signal intensity at 3000 cm^{-1} as mainly nonresonant in origin.

Representative SFG spectra acquired at 0, 5, and 20 min during CTAB adsorption are shown in Figure 6, panels A, B and C. Initially, as demonstrated in Figure 6A, a broad peak is observed. This peak is mainly attributable to the strong nonresonant background, and accordingly, the peak shape matches the intensity profile of the incident IR pulse convoluted by signal contributions from the OH stretching modes of the interfacial water molecules above 3000 cm^{-1}.[93] Note that the incident broadband IR pulse is centered at ∼2975 cm^{-1}, and the signal intensity tail-off toward 3200 cm^{-1} is due to the fact that there is no more incident IR excitation present at that frequency.

After about 5 min, the nonresonant background signal has significantly diminished, while vibrational resonances due to CTA emerge in the spectrum (Figure 6B). Figure 6B clearly shows that as positively charged CTA adsorbs to the surface,

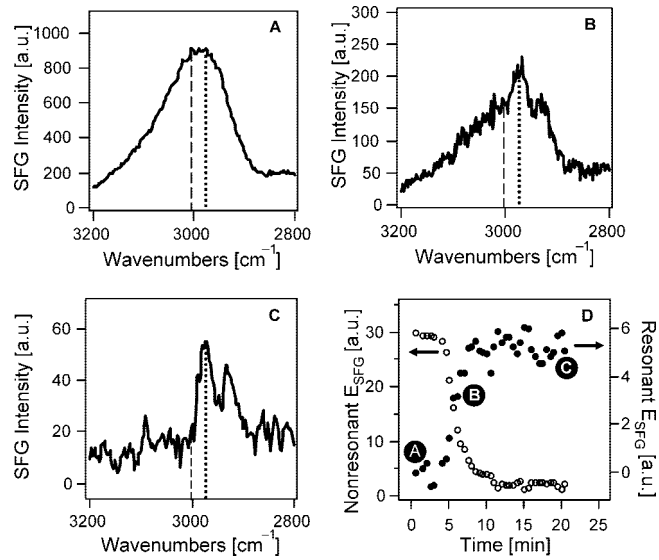

Figure 6. Time-resolved raw SFG signal from the silica/aqueous interface during the CTA adsorption process at 10 mM NaCl and 30 μM CTA. (A) Spectrum at $t = 30$ s before significant CTA adsorption has occurred. The broad peak is due to the interfacial potential, which generates a strong nonresonant signal. The peak shape follows the intensity distribution of the IR laser pulse. (B) Spectrum at $t = 330$ s where both the diminished nonresonant background and the resonant peaks due the CTA vibrational resonances are apparent. (C) Spectrum at $t = 20$ min. CTA adsorption is complete and the nonresonant background is weak. The resonant CTA vibrational modes are clearly present. (D) Change in nonresonant (empty circles) and resonant (solid circles) SFG *E*-fields during CTA adsorption to the silica/aqueous interface. The resonant signal corresponds to the asymmetric stretch of the methyl group on the ammonium headgroup. The dashed and dotted lines in each panel represent where the nonresonant and resonant signals were measured, respectively. (Note that before plotting in part D, all data were normalized to the broadband IR pulse intensity distribution, see Figure S9 in Supporting Information for normalized spectra.) The black circles with the white letters mark the time where the SFG spectra displayed in parts A−C were recorded. See text for details regarding the separation of nonresonant and resonant contributions to the SFG *E*-Field.

the nonresonant background signal decreases, which we attribute to a decrease in the interfacial potential. After approximately 20 min, the system reaches a steady state with minimal nonresonant background and distinctive C−H stretching resonances. (Figure 6C). The time-resolved SFG experiment is summarized in Figure 6D, which displays the resonant and nonresonant SFG *E*-fields, after proper subtraction of the nonresonant contribution from the resonant, obtained from SFG spectra recorded every 30 s. SFG spectra are plotted according to the time when the spectral acquisition was finished (i.e., the first spectrum acquired is plotted at $t = 30$ s).

Following an approach analogous to that utilized by Schrödle and Richmond for the case of dodecanoate interacting with the fluorite/water interface,[90] the data were normalized and correlated (Figure 7). Clearly, there is a strong negative correlation between the nonresonant signal, which tracks interfacial potential, and the resonant signal from CTA. This result is expected given that during adsorption the positive charge of the ammonium headgroup cancels the charge at the silica/aqueous interface while simultaneously the number of resonant adsorbates increases. Moreover, in Figure 7, a line with a slope of negative one is an excellent fit to the data. If CTA adsorption occurred initially with few coadsorbed counterions, and then proceeded at later times with more coadsorbed counterions, the fit in Figure 7 would be curved with an initially steeper slope.

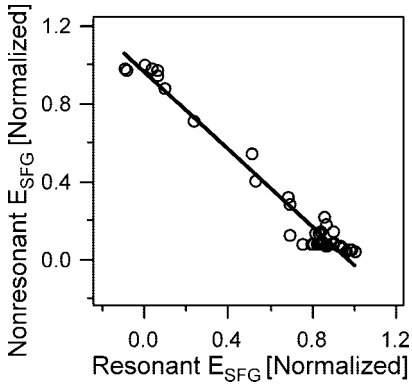

Figure 7. Normalized nonresonant *E*-field plotted versus the normalized resonant *E*-field. The solid line, with slope of negative one and *y*-intercept of one, represents an idealized linear correlation between changes in the nonresonant and resonant contributions to the SFG spectra.

Given that at later times in the adsorption process the surface charge density of the surface would be more positive and may favor greater coadsorption of counterions, this scenario is not entirely unreasonable. However, the linearity in Figure 7 instead indicates that for 10 mM NaCl and 30 μM CTAB, the ratio of counterions to surfactant molecules adsorbing to the interface is constant during the duration of CTA adsorption. Taking the potential to be linearly dependent on the surface charge density, as described by the constant capacitance model, time lags are not observed between the adsorption of CTA and counterions, which is consistent with related isotopic exchange experiments reported by Schrödle and Richmond.[90]

Figure 7 also indicates that structural rearrangement does not occur within the bound CTA during the adsorption process. If CTA rearranged into a presumably more symmetric structure such as a bilayer-like aggregate, then the increase in the resonant SFG signal corresponding to an increase in the number of adsorbates would be smaller at higher surface coverage relative to lower coverage due to cancelation of oppositely aligned vibrational modes. In this scenario, the plot in Figure 7 would again be curved except with the slope becoming steeper from left-to-right because the resonant contribution to the SFG signal would become insensitive to increasing CTA coverage due to the increased symmetry of the system (and SFG signal cancelation) at higher surface coverage. Our conclusion that structural rearrangement does not occur is not surprising given the relatively low surface coverage calculated for 30 μM CTAB ($\sim$40% of the maximum coverage) from our SHG data (vide supra). Our findings, then, are consistent with the notion that CTA is adsorbed at the silica/water interface as isolated aggregates[11] at these concentrations, and that there is little driving force for rearrangement into a more symmetric structure. Furthermore, our time-resolved SFG experiments support our earlier conclusion in section IV.B, which was made based on our thermodynamic data, that CTA adsorption occurs as a single step with electrostatic adsorption and surface aggregation occurring concurrently.

These conclusions regarding surface structure and dynamics are limited to the specific conditions investigated herein (10 mM NaCl and 30 μM CTA). However, given that the resonant SFG *E*-field is proportional to the number of adsorbates (see eq 6), our SFG results are an important alternative method to determine how the interfacial potential changes with surface coverage, and this method does not require assuming a particular electrostatic double layer model. Clearly, from Figure 7 the potential-dependent (i.e., nonresonant) SFG *E*-field is linearly dependent on resonant SFG *E*-field (i.e., surface coverage). This linear correlation is consistent with the constant-capacitance models and triple-layer models and verifies that the Eisenthal $\chi^{(3)}$ technique, which tracks interfacial potential, is an appropriate method for studying CTA adsorption. Additionally, the excellent negative correlation between nonresonant and resonant SFG *E*-fields indicates that the adsorption process leads to charge cancelation at the interface, which is expected given that CTA is a cationic surfactant.

VI. Conclusions

Through use of the Eisenthal $\chi^{(3)}$ method, we characterized the thermodynamics and electrostatics of cetyltrimethylammonium interaction with the fused silica/aqueous interface across a range of ionic strengths and at pH 11. In particular, the reversibility, binding constants, and free energies were analyzed at four NaCl concentrations: 10, 100, 300, and 500 mM. By analyzing the adsorption free energies as a function of interfacial potential at these four salt concentrations, the charge density per adsorbate was determined, indicating that CTA coadsorbs with counterions at a ratio of approximately 4 to 3 (i.e., 4 CTA^+ ions for every 3 Cl^- ions), which is similar to the ratio of counterion binding reported for bulk micelles. Furthermore, the chemical (i.e., non-Coulombic) portion of the free energy was found to dominate the overall free energy of adsorption, indicating that CTA adsorption at these ionic strengths is primarily driven by the favorable hydrophobic interactions between interdigitated surfactant hydrocarbon chains in the adsorbed aggregate. By applying the triple-layer model to our data, an average charge density of $2.8(3) \times 10^{13}$ charges/cm^2, which corresponds to 0.7 to 1.7 molecules/nm^2, was obtained for the four NaCl concentrations.

To complement the SHG experiments, the vibrational spectra of CTA and CTA-d33 at the silica/aqueous interface were characterized by using broadband SFG. In time-resolved experiments, it was demonstrated that vibrationally resonant contributions and potential dependent nonresonant background contributions to the SFG signal can be quantified simultaneously during the adsorption process, providing insight into the nonequilibrium dynamics of CTA adsorption. It was found that at 10 mM NaCl and 30 μM CTAB, little structural rearrangement of bound CTA occurs during adsorption. Furthermore, no "time lag" was found between the adsorption of CTA and counterions under our flow conditions. While this analysis required careful evaluation of the relative phase between the nonresonant and resonant *E*-fields, it should be noted that new nonresonant background suppression techniques developed by Dlott and co-workers for broadband infrared fields and narrowband upconverter fields[57,94] will facilitate future SFG studies by providing a straightforward method to separate the nonresonant and resonant signals. Clearly, the ability to simultaneously track in situ interfacial potential and vibrational resonances in adsorbates demonstrates the unique capabilities of SFG for studying surfactants at solid/liquid interfaces.

Acknowledgment. George Schatz is an inspiring scientist, excellent teacher, and most wonderful colleague whose interactions with us we cherish and celebrate with this contribution. P.L.H. acknowledges support from Schlumberger Oilfield Chemical Products and is an ARCS (Achievement Rewards for College Scientists) Foundation, Inc. Scholar, Chicago Chapter. A portion of this work was completed at the Northwestern University Integrated Molecular Structure Education and Research Center (IMSERC). A description of the facility and full

funding disclosure can be found at http://pyrite.chem.northwestern.edu/analyticalserviceslab/asl.htm. We acknowledge Spectra Physics Lasers, a division of Newport Corporation, for equipment support. We also acknowledge the International Institute for Nanotechnology (IIN) at Northwestern University for Capital Equipment support. F.M.G. acknowledges an Alfred P. Sloan fellowship and a Dow Chemical Company Professorship in Experimental Physical Chemistry.

Supporting Information Available: LC-MS calibration curves for CTA quantification, CMC determination from interfacial tension measurements of CTAB in the presence of 10, 100, 300, and 500 mM NaCl, and additional SHG and SFG plots. This material is available free of charge via the Internet at http://pubs.acs.org.

References and Notes

(1) Paria, S.; Khilar, K. C. *Adv. Colloid Interface Sci.* **2004**, *110*, 75.
(2) Chase, B.; Chmilowski, W.; Marcinew, R.; Mitchell, C.; Dang, Y.; Krauss, K.; Nelson, E.; Lantz, T.; Parham, C.; Plummer, J. *Oilfield Rev.* **1997**, *9*, 20.
(3) Sau, T. K.; Murphy, C. J. *Langmuir* **2005**, *21*, 2923.
(4) Atkin, R.; Craig, V. S. J.; Wanless, E. J.; Biggs, S. *Adv. Colloid Interface Sci.* **2003**, *103*, 219.
(5) Gu, T.; Huang, Z. *Colloids Surf.* **1989**, *40*, 71.
(6) Velegol, S. B.; Fleming, B. D.; Biggs, S.; Wanless, E. J.; Tilton, R. D. *Langmuir* **2000**, *16*, 2548.
(7) Eskilsson, K.; Yaminsky, V. V. *Langmuir* **1998**, *14*, 2444.
(8) Gutig, C.; Grady, B. P.; Striolo, A. *Langmuir* **2008**, *24*, 13814.
(9) Gutig, C.; Grady, B. P.; Striolo, A. *Langmuir* **2008**, *24*, 4806.
(10) Fragneto, G.; Thomas, R. K.; Rennie, A. R.; Penfold, J. *Langmuir* **1996**, *12*, 6036.
(11) Tyrode, E.; Rutland, M. W.; Bain, C. D. *J. Am. Chem. Soc.* **2008**, *130*, 17434.
(12) Hayes, P. L.; Malin, J. N.; Konek, C. T.; Geiger, F. M. *J. Phys. Chem. A* **2008**, *112*, 660.
(13) Konek, C. T.; Musorrafiti, M. J.; Voges, A. B.; Geiger, F. M. Tracking the Interaction of Transition Metal Ions with Environmental Interfaces Using Second Harmonic Generation. In *Adsorption of Metals by Geomedia II*; Elsevier: New York, 2007.
(14) Malin, J. N.; Hayes, P. L.; Geiger, F. M. *J. Phys. Chem. C* **2009**, *113*, 2041.
(15) Koopal, L. K.; Lee, E. M.; Boehmer, M. R. *J. Colloid Interface Sci.* **1995**, *170*, 85.
(16) Imae, T.; Ikeda, S. *Colloid Polym. Sci.* **1987**, *265*, 1090.
(17) Langmuir, D. *Aqueous Environmental Geochemistry*; Prentice-Hall, Inc.: Upper Saddle River, NJ, 1997.
(18) Morel, F. M. M.; Hering, J. G. *Principles and Applications of Aquatic Chemistry*; John Wiley & Sons: New York, 1993.
(19) Stumm, W.; Morgan, J. J. *Aquatic Chemistry, Chemical Equilibria and Rates in Natural Waters*, 3rd ed.; John Wiley & Sons: New York, 1996.
(20) Atkin, R.; Craig, V. S. J.; Biggs, S. *Langmuir* **2001**, *17*, 6155.
(21) Lindman, B.; Puyal, M. C.; Kamenka, N.; Rymden, R.; Stilbs, P. *J. Phys. Chem.* **1984**, *88*, 5048.
(22) Nevskaia, D. M.; Guerrero-Ruiz, A.; Lopez Gonzales, J. J. *Colloid Interface J.* **1998**, *205*, 97.
(23) Gibbs-Davis, J. M.; Schatz, G. C.; Nguyen, S. T. *J. Am. Chem. Soc.* **2007**, *129*, 15535.
(24) Corn, R. M.; Higgins, D. A. *Chem. Rev.* **1994**, *94*, 107.
(25) Eisenthal, K. B. *Chem. Rev.* **1996**, *96*, 1343.
(26) Heinz, T. F. Second-Order Nonlinear Optical Effects at Surfaces and Interfaces (Review Chapter). In *Nonlinear Surface Electromagnetic Phenomena*; Elsevier: Amsterdam, The Netherlands, 1991.
(27) Geiger, F. M. *Annu. Rev. Phys. Chem. (ASAP Article)* **2009**, *60*, 61.
(28) Zhao, X.; Subrahmanyan, S.; Eisenthal, K. B. *Chem. Phys. Lett.* **1990**, *171*, 558.
(29) Salafsky, J. S.; Eisenthal, K. B. *J. Phys. Chem. B* **2000**, *104*, 7752.
(30) Fitts, J. P.; Machesky, M. L.; Wesolowski, D. J.; Shang, X.; Kubicki, J. D.; Flynn, G. W.; Heinz, T. F.; Eisenthal, K. B. *Chem. Phys. Lett.* **2005**, *411*, 399.
(31) Fitts, J. P.; Shang, X.; Flynn, G. W.; Heinz, T. F.; Eisenthal, K. B. *J. Phys. Chem. B.* **2005**, *109*, 7981.
(32) Boman, F. C.; Gibbs-Davis, J. M.; Heckman, L. M.; Stepp, B. R.; Nguyen, S. T.; Geiger, F. M. *J. Am. Chem. Soc.* **2009**, *131*, 844.
(33) Boman, F. C.; Musorrafiti, M. J.; Gibbs, J. M.; Stepp, B. R.; Salazar, A. M.; Nguyen, S. T.; Geiger, F. M. *J. Am. Chem. Soc.* **2005**, *127*, 15368.
(34) Xiao, X. D.; Vogel, V.; Shen, Y. R. *Chem. Phys. Lett.* **1989**, *163*, 555.
(35) Yan, E. C. Y.; Liu, Y.; Eisenthal, K. B. *J. Phys. Chem. B* **1998**, *102*, 6331.
(36) Zhao, X.; Ong, S.; Wang, H.; Eisenthal, K. B. *Chem. Phys. Lett.* **1993**, *214*, 203.
(37) Ong, S.; Zhao, X.; Eisenthal, K. B. *Chem. Phys. Lett.* **1992**, *191*, 327.
(38) Duval, Y.; Mielczarski, J. A.; Pokrovsky, O. S.; Mielczarski, E.; Ehrhardt, J. J. *J. Phys. Chem. B* **2002**, *106*, 2937.
(39) Adamson, A. W. *Physical Chemistry of Surfaces*, 5th ed.; John Wiley & Sons: New York, 1990.
(40) Atkins, P.; de Paula, J. *Physical Chemistry*, 7th ed.; W. H. Freeman and Company: New York, 2002.
(41) Gibbs-Davis, J. M.; Kruk, J. J.; Konek, C. T.; Scheidt, K. A.; Geiger, F. M. *J. Am. Chem. Soc.* **2008**, *130*, 15444.
(42) Masel, R. I. *Principles of Adsorption and Reaction on Solid Surfaces*; John Wiley & Sons: New York, 1996.
(43) Somorjai, G. A. *Introduction to Surface Chemistry and Catalysis*; John Wiley & Sons: New York, 1994.
(44) Shen, Y. R. *The Principles of Nonlinear Optics*; John Wiley & Sons: New York, 1984.
(45) Zhu, X. D.; Suhr, H.; Shen, Y. R. *Phys. Rev. B: Condens. Matter* **1987**, *35*, 3047.
(46) Boyd, R. W. *Nonlinear Optics*, 2nd ed.; Academic Press: New York, 2003.
(47) Gopalakrishnan, S.; Liu, D.; Allen, H. C.; Kuo, M.; Shultz, M. J. *Chem. Rev.* **2006**, *106*, 1155.
(48) Richmond, G. L. *Chem. Rev.* **2002**, *102*, 2693.
(49) Shen, Y. R.; Ostroverkhov, V. *Chem. Rev.* **2006**, *106*, 1140.
(50) Moad, A. J.; Simpson, G. J. *J. Phys. Chem. A* **2005**, *109*, 1316.
(51) Richter, L. J.; Petralli-Mallow, T. P.; Stephenson, J. C. *Opt. Lett.* **1998**, *23*, 1594.
(52) Eliel, E. R.; van der Ham, E. W. M.; Vrehen, Q. H. F.; t'Hooft, G. W.; Barmentlo, M.; Auerhammer, J. M.; van der Meer, A. F. G.; van Amersfoort, P. W. *Appl. Phys. A: Mater. Sci. Process.* **1995**, *60*, 113.
(53) Hommel, E. L.; Allen, H. C. *Anal. Sci.* **2001**, *17*, 137.
(54) Schaller, R. D.; Johnson, J. C.; Wilson, K. R.; Lee, L. F.; Haber, L. H.; Saykally, R. J. *J. Phys. Chem. B.* **2002**, *106*, 5143.
(55) Bordenyuk, A. N.; Jayathilake, H.; Benderskii, A. V. *J. Phys. Chem. B.* **2005**, *109*, 15941.
(56) Rao, Y.; Comstock, M.; Eisenthal, K. B. *J. Phys. Chem. B* **2006**, *110*, 1727.
(57) Lagutchev, A.; Hambir, S. A.; Dlott, D. D. *J. Phys. Chem. C* **2007**, *111*, 13645.
(58) Wurpel, G. W. H.; Sovago, M.; Bonn, M. *J. Am. Chem. Soc.* **2007**, *129*, 8420.
(59) Fourkas, J. T.; Walker, R. A.; Can, S.; Gershgoren, E. *J. Phys. Chem. C* **2007**, *111*, 8902.
(60) Neipert, C.; Space, B. *J. Chem. Phys.* **2006**, *125*, 224706.
(61) Mifflin, A. L.; Gerth, K. A.; Geiger, F. M. *J. Phys. Chem. A* **2003**, *107*, 9620.
(62) Mifflin, A. L.; Gerth, K. A.; Weiss, B. M.; Geiger, F. M. *J. Phys. Chem. A* **2003**, *107*, 6212.
(63) Hayes, P. L.; Gibbs-Davis, J. M.; Musorrafiti, M. J.; Mifflin, A. L.; Scheidt, K. A.; Geiger, F. M. *J. Phys. Chem. C.* **2007**, *111*, 8796.
(64) Hirose, C. N. A.; Domen, K. *Appl. Spectrosc.* **1992**, *46*, 1051.
(65) Stokes, G. Y.; Buchbinder, A. M.; Gibbs-Davis, J. M.; Scheidt, K. A.; Geiger, F. M. *J. Phys. Chem. A* **2008**, *112*, 11688.
(66) Stokes, G. Y.; Buchbinder, A. M.; Gibbs-Davis, J. M.; Scheidt, K. A.; Geiger, F. M. *Vib. Spectrosc.* In press.
(67) Wang, H.-F.; Gan, W.; Lu, R.; Rao, Y.; Wu, B.-H. *Int. Rev. Phys. Chem.* **2005**, *24*, 191.
(68) Voges, A. B.; Stokes, G. Y.; Gibbs-Davis, J. M.; Lettan, R. B.; Bertin, P. A.; Pike, R. C.; Nguyen, S. T.; Scheidt, K. A.; Geiger, F. M. Invited Feature Article in *J. Phys. Chem. C* **2007**, *111*, 1567.
(69) Wang, J.; Chen, C.; Buck, S. M.; Chen, Z. *J. Phys. Chem. B* **2001**, *105*, 12118.
(70) Stokes, G. Y.; Gibbs-Davis, J. M.; Boman, F. C.; Stepp, B. R.; Condie, A. G.; Nguyen, S. T.; Geiger, F. M. *J. Am. Chem. Soc.* **2007**, *129*, 7492.
(71) Voges, A. B.; Al-Abadleh, H. A.; Musorrafiti, M. J.; Bertin, P. A.; Nguyen, S. T.; Geiger, F. M. *J. Phys. Chem. B.* **2004**, *108*, 18675.
(72) Esenturk, O.; Walker, R. A. *J. Phys. Chem. B* **2004**, *108*, 10631.
(73) Im, S. H.; Jeong, Y. H.; Ryoo, J. J. *Anal. Chim. Acta* **2008**, *619*, 129.
(74) Gonzalez, S.; Barcelo, D.; Petrovic, M. *TrAC, Trends Anal. Chem.* **2007**, *26*, 116.
(75) Ferrer, I.; Furlong, E. T. *Environ. Sci. Technol.* **2001**, *35*, 2583.
(76) Brady, P. V.; Walther, J. V. *Chem. Geol.* **1990**, *82*, 253.
(77) Al-Abadleh, H. A.; Mifflin, A. L.; Bertin, P. A.; Nguyen, S. T.; Geiger, F. M. *J. Phys. Chem. B.* **2005**, *109*, 9691.

(78) Boman, F. C.; Musorrafiti, M. J.; Gibbs, J. M.; Stepp, B. R.; Salazar, A. M.; Nguyen, S. T.; Geiger, F. M. *J. Am. Chem. Soc.* **2005**, *127*, 15368.
(79) Konek, C. T.; Musorrafiti, M. J.; Al-Abadleh, H. A.; Bertin, P. A.; Nguyen, S. T.; Geiger, F. M. *J. Am. Chem. Soc.* **2004**, *126*, 11754.
(80) Sverjensky, D. A.; Fukushi, K. *Environ. Sci. Technol.* **2006**, *40*, 263.
(81) Bartet, D.; Gamboa, C.; Sepulveda, L. *J. Phys. Chem.* **1980**, *84*, 272.
(82) Somasundaran, P.; Healy, T. W.; Fuerstenau, D. W. *J. Phys. Chem.* **1964**, *68*, 3562.
(83) Ersoy, B.; Celik, M. S. *Clays Clay Miner.* **2003**, *51*, 172.
(84) Bryleva, E. Y.; Vodolazkaya, N. A.; McHedlov-Petrossyan, N. O.; Samokhina, L. V.; Matveevskaya, N. A.; Tolmachev, A. V. *J. Colloid Interface Sci.* **2007**, *316*, 712.
(85) Geiger, F. M.; Pibel, C. D.; Hicks, J. M. *J. Phys. Chem. A* **2001**, *105*, 4940.
(86) Corn, R. M.; Higgins, D. A. *Chem. Rev.* **1994**, *94*, 107.
(87) Steel, W. H.; Walker, R. A. *Nature* **2003**, *424*, 296.
(88) Konek, C. T.; Illg, K. D.; Al-Abadleh, H. A.; Voges, A. B.; Yin, G.; Musorrafiti, M. J.; Schmidt, C. M.; Geiger, F. M. *J. Am. Chem. Soc.* **2005**, *127*, 15771.
(89) Petersen, P. B.; Saykally, R. J. *Annu. Rev. Phys. Chem.* **2006**, *57*, 333.
(90) Schroedle, S.; Richmond, G. L. *J. Am. Chem. Soc.* **2008**, *130*, 5072.
(91) Campbell, R. A.; Parker, S. R. W.; Day, J. P. R.; Bain, C. D. *Langmuir* **2004**, *20*, 8740.
(92) Wang, W.; Gu, B.; Liang, L.; Hamilton, W. A. *J. Phys. Chem. B* **2004**, *108*, 17477.
(93) Ostroverkhov, V.; Waychunas, G. A.; Shen, Y. R. *Phys. Rev. Lett.* **2005**, *94*, 046102.
(94) Carter, J. A.; Wang, Z.; Dlott, D. D. *J. Phys. Chem. A* **2008**, *112*, 3523.

JP810891V